Supporting Information

Plasmon-Enhanced Catalysis: Distinguishing Thermal and Non-Thermal Effects

Xiao Zhang,[1] Xueqian Li,[1] Matthew E. Reish,[2] Du Zhang,[1] Neil Qiang Su,[1] Yael Gutiérrez,[3] Fernando Moreno,[3] Weitao Yang,[1,4] Henry O. Everitt,[2,4] Jie Liu[1]

[1]*Department of Chemistry, Duke University, Durham, NC 27708*

[2]*Army Aviation & Missile RD&E Center, Redstone Arsenal, AL 35898*

[3]*Optics Group, Department of Applied Physics, University of Cantabria, Avda de Los Castros, s/n 39005 Santander, Spain*

[4]*Department of Physics, Duke University, Durham, NC 27708*

Reaction mechanism and rate law

The first step of CO_2 hydrogenation to produce CH_4 (CO_2 methanation) on Rh and Ru catalysts is idenfied to be dissociative adsorption of CO_2 as CO* and O*. H_2 also readily dissociatively adsorbed as H*. However, the sequence of CO* hydrogenation and C-O bond dissociation is still under debate, *i.e.*, C-O bond dissociation could happen in CO, CHO and CH_2O intermediates. The possible reaction mechanisms and corresponding rate equations are shown below.

CHO intermediate mechanism

1. $CO_{2(g)} + 2\ * \rightleftharpoons CO^* + O^*$
2. $H_{2(g)} + 2\ * \rightleftharpoons 2\ H^*$
3. $CO^* + H^* \rightleftharpoons CHO^* + *$
4. $CHO^* + * \rightleftharpoons CH^* + O^*$
5. $O^* + H^* \rightleftharpoons OH^* + *$
6. $OH^* + H^* \longrightarrow H_2O_{(g)} + 2\ *$
7. $CH^* + H^* \rightleftharpoons CH_2^* + *$
8. $CH_2^* + H^* \rightleftharpoons CH_3^* + *$
9. $CH_3^* + H^* \longrightarrow CH_{4(g)} + 2\ *$

Step 4 (CH-O dissociation) as RDS:

$$R = \frac{(K_1K_3K_5k_4k_6/2)^{1/2}K_2^{\,3/4}}{\left[1 + K_2^{\,1/2}P_{H2}^{\,1/2} + \left(K_1K_2^{\,1/2}K_5k_6/2K_3k_4\right)^{1/2}P_{CO2}^{\,1/2}P_{H2}^{\,1/4}\right]^2} P_{CO2}^{\,1/2}P_{H2}^{\,3/4}$$

Step 3 (CHO formation) as RDS:

$$R = \frac{(K_1K_5k_3k_6/2)^{1/2}K_2^{\,3/4}}{\left[1 + K_2^{\,1/2}P_{H2}^{\,1/2} + \left(K_1K_2^{\,1/2}K_5k_6/2k_3\right)^{1/2}P_{CO2}^{\,1/2}P_{H2}^{\,1/4}\right]^2} P_{CO2}^{\,1/2}P_{H2}^{\,3/4}$$

CH_2O intermediate mechanism

1. $CO_{2(g)} + 2\ * \rightleftharpoons CO^* + O^*$
2. $H_{2(g)} + 2\ * \rightleftharpoons 2\ H^*$
3. $CO^* + H^* \rightleftharpoons CHO^* + *$
4. $CHO^* + H^* \rightleftharpoons CH_2O^* + *$
5. $O^* + H^* \rightleftharpoons OH^* + *$
6. $OH^* + H^* \longrightarrow H_2O_{(g)} + 2\ *$
7. $CH_2O^* + * \rightleftharpoons CH_2^* + O^*$
8. $CH_2^* + H^* \rightleftharpoons CH_3^* + *$
9. $CH_3^* + H^* \longrightarrow CH_{4(g)} + 2\ *$

Step 7 (CH_2-O dissociation) as RDS:

$$R = \frac{(K_1K_3K_4K_5k_6k_7)^{1/2}K_2}{\left[1 + {K_2}^{1/2}{P_{H2}}^{1/2} + (K_1K_5k_6/2K_3K_4k_7)^{1/2}{P_{CO2}}^{1/2}\right]^2}{P_{CO2}}^{1/2}P_{H2}$$

CO intermediate mechanism

1. $CO_{2(g)} + 2\,* \rightleftharpoons CO^* + O^*$
2. $H_{2(g)} + 2\,* \rightleftharpoons 2\,H^*$
3. $CO^* + * \rightleftharpoons C^* + O^*$
4. $C^* + H^* \rightleftharpoons CH^* + *$
5. $O^* + H^* \rightleftharpoons OH^* + *$
6. $OH^* + H^* \longrightarrow H_2O_{(g)} + 2\,*$
7. $CH^* + H^* \rightleftharpoons CH_2^* + *$
8. $CH_2^* + H^* \rightleftharpoons CH_3^* + *$
9. $CH_3^* + H^* \longrightarrow CH_{4(g)} + 2\,*$

Step 3 (C-O dissociation) as RDS:

$$R = \frac{(K_1K_2K_5k_3k_6/2)^{1/2}}{\left[1 + {K_2}^{1/2}{P_{H2}}^{1/2} + (K_1K_2K_5k_6/2k_3)^{1/2}{P_{CO2}}^{1/2}{P_{H2}}^{1/2}\right]^2}{P_{CO2}}^{1/2}{P_{H2}}^{1/2}$$

Step 4 (C hydrogenation) as RDS:

$$R = \frac{(K_1K_3{K_5}^2k_4{k_6}^2)^{1/3}{K_2}^{5/6}}{\left[1 + {K_2}^{1/2}{P_{H2}}^{1/2} + \left({K_1}^2K_5k_6/2K_3k_4\right)^{1/3}{K_2}^{1/6}{P_{CO2}}^{2/3}{P_{H2}}^{1/6}\right]^2}{P_{CO2}}^{1/3}{P_{H2}}^{5/6}$$

The smallest reaction order on H_2 is -0.5 (CO intermediate mechanism with step 3, C-O dissociation as RDS), bigger than the observed reaction order on H_2 of -1.24 for the hot-electron-driven reaction.

Example of iterative calculation of the equivalent temperature and apparent activation energy

With a thin layer of Rh-s/TiO_2 catalyst (~1 mm thickness), the top- and bottom-surface temperatures and thermal reaction rate in dark are listed in the table below:

Table S1

T_1/°C	T_2/°C	R_t/μmol g^{-1} s^{-1}	s.d.
325	344	216.2	1.1
300	323	119.1	1.5
275	299	59.7	0.2
250	272	26.0	0.1
225	245	10.9	0.1
200	217	3.97	0.07
175	190	1.33	0.06
150	163	0.38	0.04

Under constant partial pressures of reactants, the relationship between reaction rate (r in μmol g^{-1} s^{-1}) and temperature (T in K) can be described by Arrhenius equation:

$$\ln(r) = \frac{-E_a}{R}\left(\frac{1}{T}\right) + \ln(A)$$

The apparent activation energy, E_a, can be obtained by linear fitting of ln(r) to 1/T with least squares method.

Using T_1 as T, E_a is calculated to be 76.8±1.3 kJ/mol. Using T_2 as T, E_a is calculated to be 78.0±1.3 kJ/mol. The difference in activation energies is due to the different top- and bottom-surface temperatures of catalyst bed. As a result, an equivalent temperature, T_e, should be used to consider the temperature gradient that exists within the catalyst bed.

Assuming a uniform temperature gradient model, the equation to calculate the equivalent temperature is shown as follows:

$$e^{\frac{-E_a}{RT_e}} = \frac{1}{T_2 - T_1}\int_{T_1}^{T_2} e^{\frac{-E_a}{RT}}\, dT$$

Due to the recursive nature of this calculation, an initial E_a is used and an iterative method is used to get the real E_a.

Iteration 1: Using the input E_a (76.8±1.3 kJ/mol) calculated with T_1, the following equivalent temperatures are obtained:

Table S2

T_e/°C	T_1/°C	T2/°C
334.8	325	344
312.0	300	323
287.6	275	299
261.6	250	272
235.5	225	245
208.9	200	217
182.9	175	190
156.8	150	163

E_a = 77.4±0.1 kJ/mol

Iteration 2: Input Ea = 77.4±0.1 kJ/mol

Table S3

T_e/°C	T_1/°C	T2/°C
334.8	325	344
312.0	300	323
287.6	275	299
261.6	250	272
235.5	225	245
208.9	200	217
182.9	175	190
156.8	150	163

E_a = 77.5±0.1 kJ/mol

Both E_a and T_e converge and the calculation is complete.

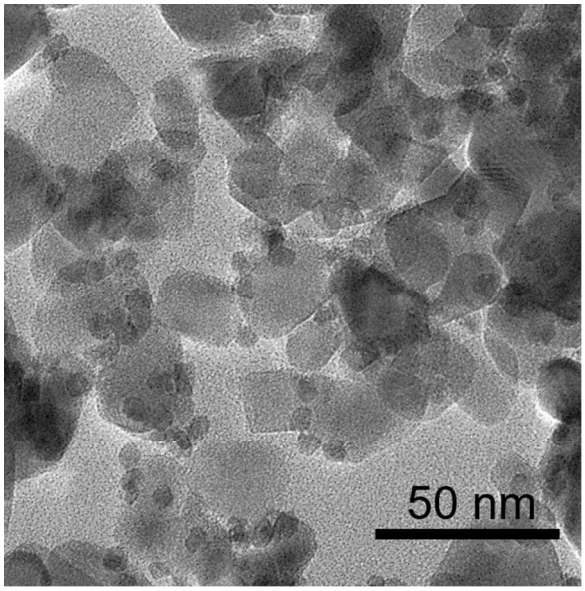

Figure S1. Representative TEM image of 6 nm spherical rhodium nanoparticles supported on titanium dioxide (Rh-s/TiO_2).

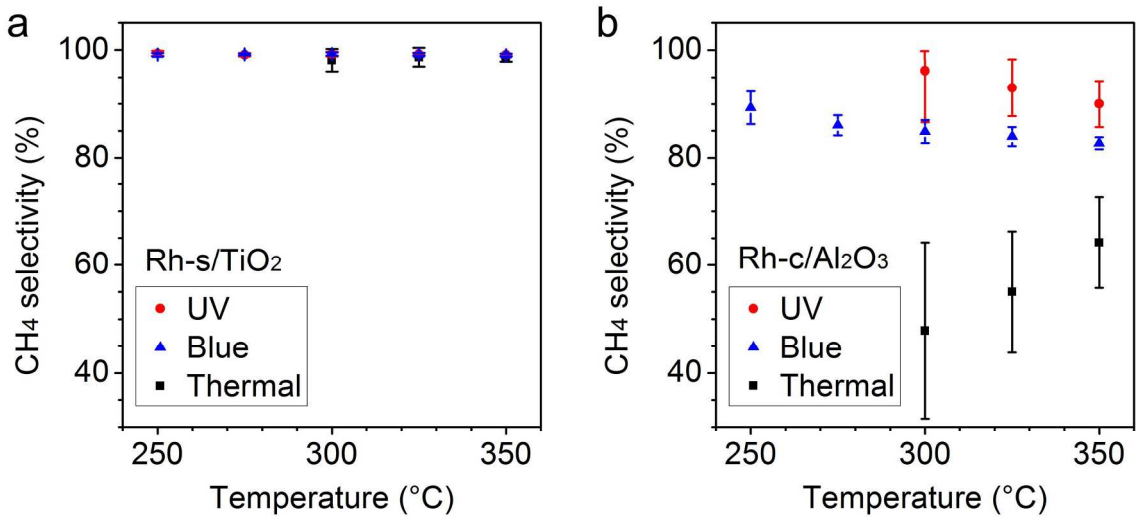

Figure S2. Selectivity towards CH_4 in dark (black squares) and under 2.8 W cm^{-2} UV (red circles) and blue (blue triangles) illumination as a function of chamber temperature on TiO_2 supported Rh spheres (a, Rh-s/TiO_2) and Al_2O_3 supported Rh cubes (b, Rh-c/Al_2O_3). The reactions are carried out with 50 sccm CO_2, 150 sccm H_2, and 50 sccm Ar. Error bars represent the s.d. of measurements by the mass spectrometer.

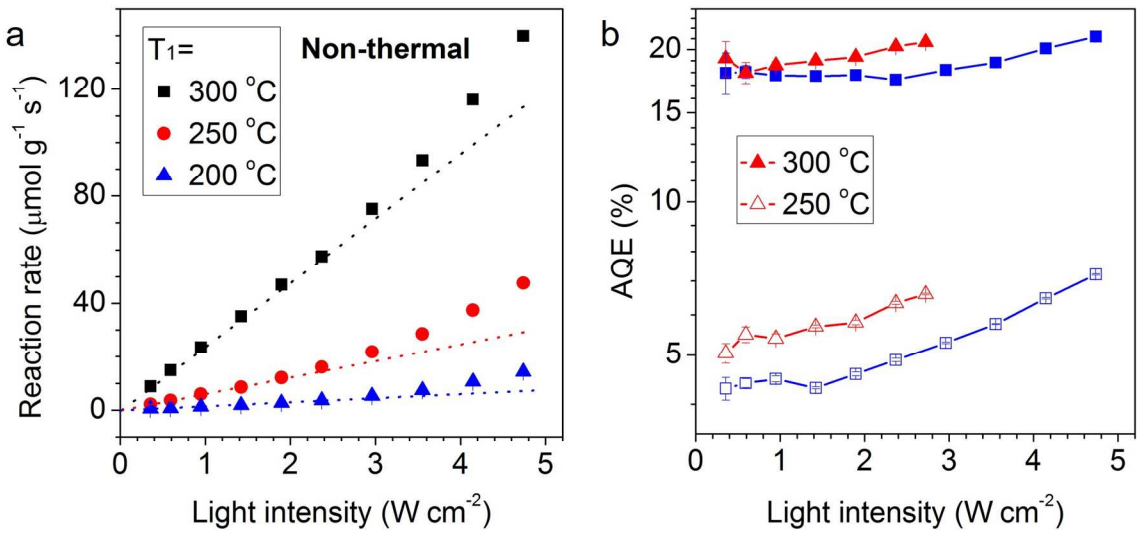

Figure S3. a, Non-thermal CH_4 production rates on the Rh-s/TiO_2 catalyst at top-surface temperature of 300 °C (black squares), 250 °C (red circles), and 200 °C (blue triangles) as a function of blue light intensity. The dependence of non-thermal reaction rates on light intensity shows a super-linear increase with light intensity. b, AQE of plasmon-enhanced CO_2 methanation on the Rh-s/TiO_2 catalyst under UV (red triangles) and blue (blue squares) illumination at top-surface temperature of 300 °C (solid symbols) and 250 °C (open symbols). The reaction under blue light shows slightly lower AQE than that under UV light at the same light intensity. The reactions are carried out with 50 sccm CO_2, 150 sccm H_2, and 50 sccm Ar. Error bars represent the s.d. of measurements by the mass spectrometer.

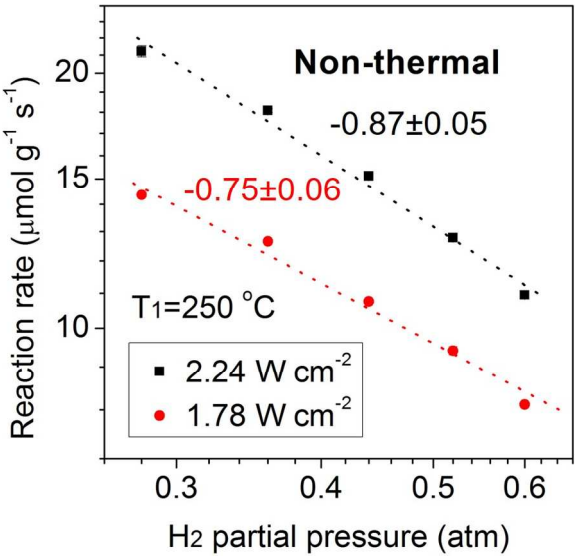

Figure S4. Non-thermal reaction rate as a function of H_2 partial pressure under 2.24 (black squares) and 1.78 W cm^{-2} (red circles) UV illumination at top-surface temperature of 250 ^{o}C. The non-thermal reaction rate under UV illumination shows the same decreasing trend with increasing H_2 partial pressure as that under blue illumination. The CO_2 flow rate is fixed at 40 sccm with varying H_2 and Ar flow rates to maintain a total flow rate of 250 sccm. Error bars represent the s.d. of measurements by the mass spectrometer.

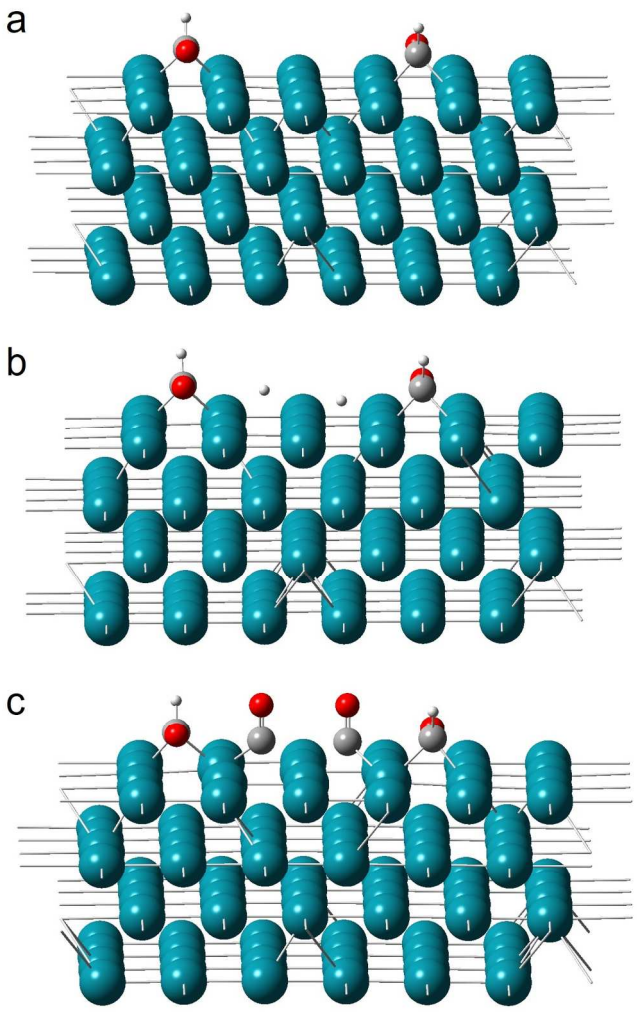

Figure S5. Side view of optimized configurations of two CHO adsorbates on Rh(100) facet separated by 2 Rh surface atoms with bare Rh surface (a), 2 H atoms (b), and 2 CO molecules (c) in between for calculations of LDOS of the C-O anti-bonding orbitals. The dark cyan, gray, red, and white spheres are Rh, C, O, and H atoms, respectively. x axis is perpendicular to the Rh surface and y axis is parallel to the C-O bond in CHO adsorbates.

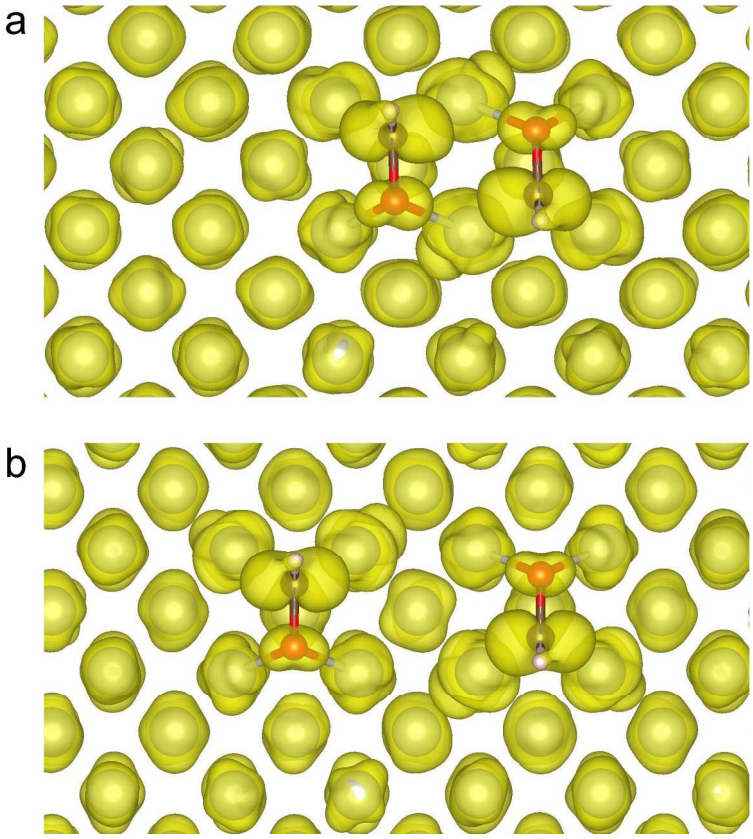

Figure S6. Top view of distribution of C-O anti-bonding orbitals consisting of two CHO adsorbates on Rh(100) facet at adjunct Rh surface atoms (a) and separated by one Rh atom (b). The delocalization of C-O anti-bonding orbitals is shown as the evenly distributed probability density among the two CHO intermediates.

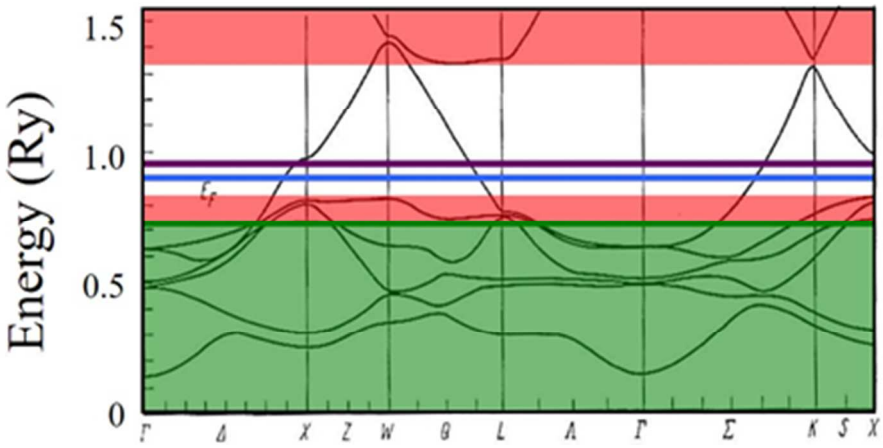

Figure S7. The band diagrams of rhodium (modified from *phys. stat. sol. (b)*, 1973, 55, 117 for review only). The green regions represent the filled bands up to the Fermi energy; the red bands are the parasitic interband absorption regions; the blue and violet bands represent the photon energies we used. Note the energy unit in the Y axis of Rh band structure is Rydberg (1Ry~13.6 eV).

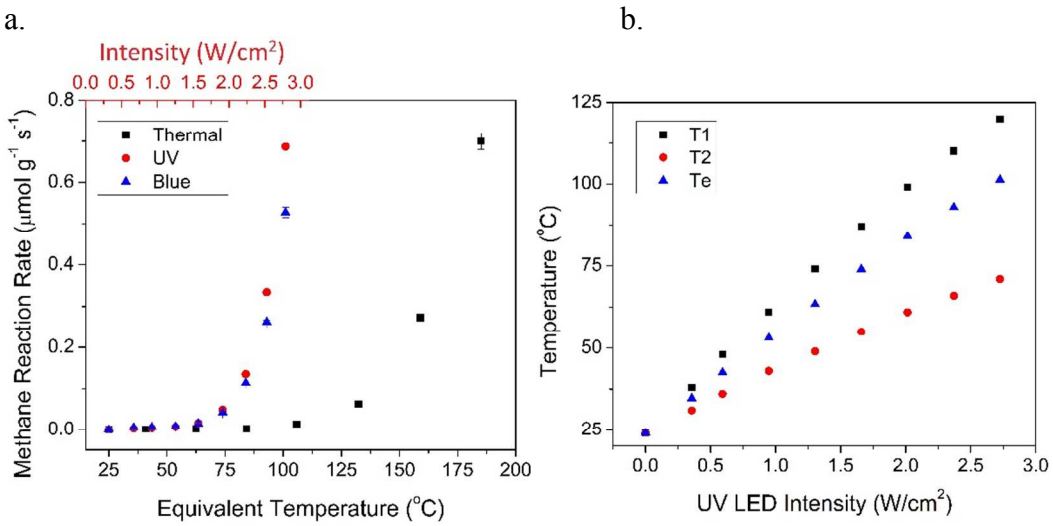

Figure S8. (a) Methane reaction rates of dark thermal conditions, and light UV/Blue conditions at low temperatures as a function of equivalent temperature. Top secondary x-axis represents corresponding intensity of UV/Blue LED. (b) Measured top-surface (T_1), bottom-surface (T_2) and calculated equivalent (T_e) temperatures of the catalyst bed under illumination of the UV LED. The reactions are carried out with 50 sccm CO_2, 150 sccm H_2, and 50 sccm Ar. Some error bars are smaller than symbols and represent the s.d. of measurements by the mass spectrometer.